Dynamic Analysis of a Flexible Beam Undergoing Reciprocating Rotational Motion

X. Wang[1], R.G. Langlois[1], M.J.D. Hayes[1]

[1] *Department of Mechanical & Aerospace Engineering, Carleton University, 1125 Colonel By Drive, Ottawa, ON, K1S 5B6, Canada*
xbwang@connect.carleton.ca
xiaobin@hotmail.com
rlangloi@mae.carleton.ca
jhayes@mae.carleton.ca

In this paper the dynamic characteristics of a flexible beam are determined experimentally and compared with those predicted by a simulation. A set of static experiments is first performed to validate the beam parameters and the experimental measurement approach. Next, the beam is set into motion as the rocker link of a planar four-bar crank-rocker linkage driven by a DC motor. Strain gauges, a potentiometer, and data acquisition system are employed to obtain measurements of the beam position history and corresponding strains during motion. From the signal analysis and data fit, the deflection and curvature of the flexible beam are determined. The simulation is carried out in ADAMS by creating a model with the same configuration and boundary conditions. The results of the experiment and simulation are closely matched. The long-term goal of this work is to develop practical means for continuous measurement of beam curvature and associated tip deflection and using that information to improve tip positioning control.

1 INTRODUCTION

Flexibility is an inherent property of structural members. It becomes one of major concern when mechanical systems are designed with tight shape and dimension tolerances, required to be lighter in weight, and to move at higher speeds effectively negating the rigid body assumption. In addition there are many applications that use deformations, and corresponding strengths of structural members, to assemble machine components and avoid interference among parts, for example, *selectively compliant assembly robot arms* (SCARA). The dynamic characteristics of flexible beams, such as deflection under inertial loading, are closely related to their material properties, geometry, and boundary conditions. Hence, a mathematical model and measurement system are required to experimentally determine characteristics of interest.

In this paper, we investigate the dynamic performance of flexible bodies using dynamic simulation, wherein the beam has been suitably modelled, and empirical data has been collected to confirm the simulation. The experimental apparatus, illustrated in Figure 1, consists of the following elements. A commercially available long and slender aluminum beam is used as the flexible body. Strain gauges, mounted in strategic locations parallel to the longitudinal beam axis, are used to measure motion-induced strain. A motor driven four-bar crank-rocker linkage provides oscillating rotations for the beam. A precision potentiometer is used to measure the rocker link orientation. The beam is rigidly clamped to the relatively stiff rocker. The computer-controlled data acquisition system is used to acquire simultaneous signals from four strain gauges and the potentiometer when the beam is in motion. The simulation is developed using the ADAMS software package. The same configurations and conditions for the experiment are modelled and recreated in the simulation. The data from the measurement system and simulation are analyzed and compared. The curvature of the beam as a function of distance along the beam from the clamp is obtained. It is shown that the simulation and empirical results are reasonably well matched.

One application of these results is the ability to predict beam curvature, at any location along the beam, given the angular position and velocity of the actuator. Another, perhaps more important one is the ability to use the strain gauge and potentiometer outputs as feedback control to the motor for controlling the shape of the beam at specific

angular positions.

2 STATIC ANALYSIS

2.1 Experiment

The long slender flexible beam is a commercially available aluminum plate 3.18 $\times$ 19.05 $\times$ 914.4 mm. Four 120Ω $\pm 0.3\%$ strain gauges were bonded to the beam so their direction of sensitivity is aligned with the longitudinal axis of the beam. The flexible beam was cantilevered to the rocker link of a planar crank-rocker mechanism such that the beam was flexible in a plane parallel to the floor (perpendicular to the gravity vector, to mitigate its effects). The potentiometer was attached to the base-fixed revolute joint so as to measure its angular position. The crank was driven by a geared-down DC motor. The four strain gauges were located at distances $[5, 204, 403, 603]$ mm along the beam measured from the clamped end mounted to the rocker. The effective length of the flexible beam is 835 mm. The mechanism configuration and strain gauge locations are shown pictorially and schematically in Figures 1 and 2, respectively.

A static test and calculation were performed to verify the setup. In order to compare measured and simulated results in the dynamic case, a measurement approach using the strain gauges to estimate the dynamic beam tip deflection is required. Consequently, a series of static tests were performed to validate the measurement approach and to compare its result with alternative methods for obtaining the tip deflection. For this purpose, the beam was removed from the crank-rocker mechanism and set up such that it would bend in a vertical plane as the result of weights associated with masses of different magnitude suspended from the free end of the beam. The corresponding strains and tip displacements were measured under the effect of the applied loads.

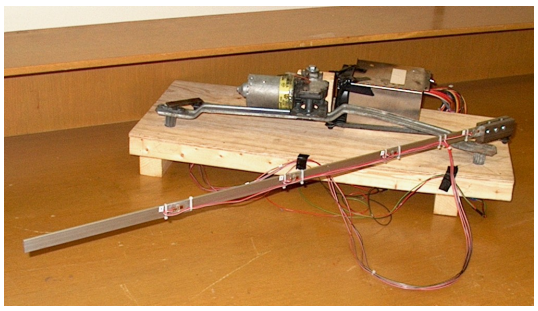

Figure 1: Experimental apparatus

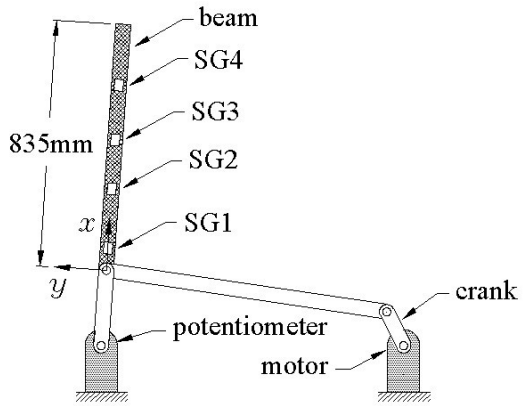

Figure 2: Schematic illustration of mechanism configuration and strain gauge attachment points

2.2 Direct Measurement

For each of the three masses used, repeated reading of a precision ruled straight edge were used to directly measure the difference between the vertical position of the beam tip prior to application of the tip weights and the deflected positions once the weights were attached and the system was allowed to settle to equilibrium. The directly measured deflections are provided in Table 1.

2.3 Theoretical Calculation

Knowing the material properties, geometry, and applied tip loads, a simple beam bending calculation was performed to ensure consistency between the beam parameters and the physical reality of the system. The beam tip deflection was calculated [1] for each of the three known tip weights using

$$\delta = \frac{1}{3}\frac{PL^3}{EI}, \tag{1}$$

where E is Young's modulus for the beam material, I is the area moment of inertia of the beam, δ is the deflection of the free end, P is the magnitude of the applied force (weight), and L is the distance between the force application point and the beam cantilever point. The three calculated tip deflection results are provided in Table 1.

2.4 Computational Estimate

Beam bending theory [1] relates beam surface strain, applied bending moment, and beam curvature such that

$$\frac{d^2y}{dx^2} = \frac{\varepsilon}{h} = \frac{M}{EI}, \tag{2}$$

Table 1: Strains (micro) and tip displacement (mm) associated with tip mass (kg)

	Strain 1	Strain 2	Strain 3	Strain 4	Tip Displacement	Mass
Measurement	191.00	143.00	96.00	52.00	26.99	0.05129
Calculation	186.63	141.34	96.05	50.53	26.84	
Estimation	190.69	143.35	96.76	50.71	27.226	
Simulation	184.12	140.37	95.03	50.09	24.59	
Measurement	361.00	272.00	185.00	100.00	51.59375	0.09966
Calculation	362.64	274.64	186.63	98.18	52.14	
Estimation	360.35	273.04	185.76	98.08	51.86	
Simulation	356.50	272.75	184.65	97.33	49.27	
Measurement	534.00	403.00	276.00	148.00	78.18	0.1478
Calculation	537.82	407.30	276.78	145.60	77.33	
Estimation	533.01	404.90	276.14	146.08	76.90	
Simulation	530.57	404.49	273.85	144.34	73.84	

where

$$M = (L - x)P \tag{3}$$

and y is the deflection of the beam along its length x from the clamped end, ε is strain, h is the distance from the centreline to the surface of the beam, and M is the bending moment present at position x along the beam.

Consequently, using the known tip weights, it is possible to integrate the beam curvature calculated from Equation 2 to predict the shape of the deflected beam and ultimately the tip deflection. While possible, this approach would not directly contribute to the required measurement approach as in the dynamic situation, the inertial loading along the length of the beam will not be known a priori. Consequently, instead, the measured strains at four locations were used to calculate the beam curvature. This data was then curve fitted along the length of the beam, and integrated, using appropriate boundary conditions, to obtain the beam deflected shape and tip deflection. Results are presented in Table 1. This approach is similar to what is presented in Reference [2].

2.5 Transient Simulation

A dynamic flexible body simulation of the crank-rocker mechanism and flexible beam was developed using the ADAMS multibody dynamics software package. The flexible beam was meshed automatically using parabolic tetrahedral elements ranging in size from 3 mm to 5 mm along their edges. ADAMS uses the conventional modal superposition approach for simulating linear deformation of flexible bodies [3]. The six lowest-frequency vibration modes were included in the simulation. To verify and validate the dynamic simulation using the static data, transient dynamic simulations were run for each of the static loading cases and the resulting steady-state strains and tip deflections are presented in Table 1. Figure 3 shows a sample of the deflected shape of the beam compared with the undeflected beam configuration. Figure 4 shows the corresponding levels of strain where, in this case, x is measured inboard from the beam tip.

Figure 3: Deformed beam shape predicted by ADAMS simulation

2.6 Static Results

Inspection of the summary results presented in Table 1 shows excellent agreement between the measured, calculated, predicted, and simulated strains for the three static load cases considered. In general, the simulated results produced the lowest tip deflections and those farthest from the directly measured values, though the difference was limited to 4.5% to 9% based on the measured values. The general agreement between the predicted and measured values validates the use of the measured strains as an effective means for measuring the beam deformation along the length and the instantaneous tip deflection.

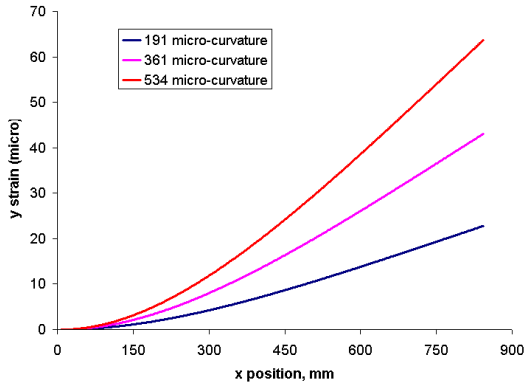

Figure 4: Surface strain versus position for the static load cases where x is measured positive moving inboard from the beam tip

3 DYNAMIC ANALYSIS

3.1 Test Conditions

As described previously, for the dynamic testing, the beam was mounted to the follower link of the four-bar linkage using a rigid hub. A precision potentiometer was used to continuously measure the orientation of the follower link. A data acquisition system was configured to sample the follower orientation and the strains at each of the four locations. The sampling rate was set to 400 Hz; and a Butterworth filter was used with the pass band set to 150 Hz and the stop band set at 200 Hz. While the apparatus allows the mechanism to be operated over a range of speeds, the data presented herein corresponds to an excitation frequency of the mechanism crank of 0.92 Hz. A set of recorded time history data from the potentiometer and four strain gauges is shown in Figure 5. The frequency spectrum of the strain measured at strain gauge 1 is shown in Figure 6. The two largest peaks in the spectrum correspond to the rotation frequency of 0.92 Hz (largest peak) and the first natural frequency of the beam at 3.56 Hz (second-largest peak). Peaks at frequencies in the area of the second and higher natural vibration frequencies for the beam are very small. Several harmonics of the excitation frequency seem to be present, which could indicate a periodic, but non-sinusoidal excitation.

Inspection of Figure 5 reveals the expected results that the strain amplitude cycles are in phase with the angular excitation of the system and that the strain amplitudes decrease for locations further away from the cantilever point. It is also

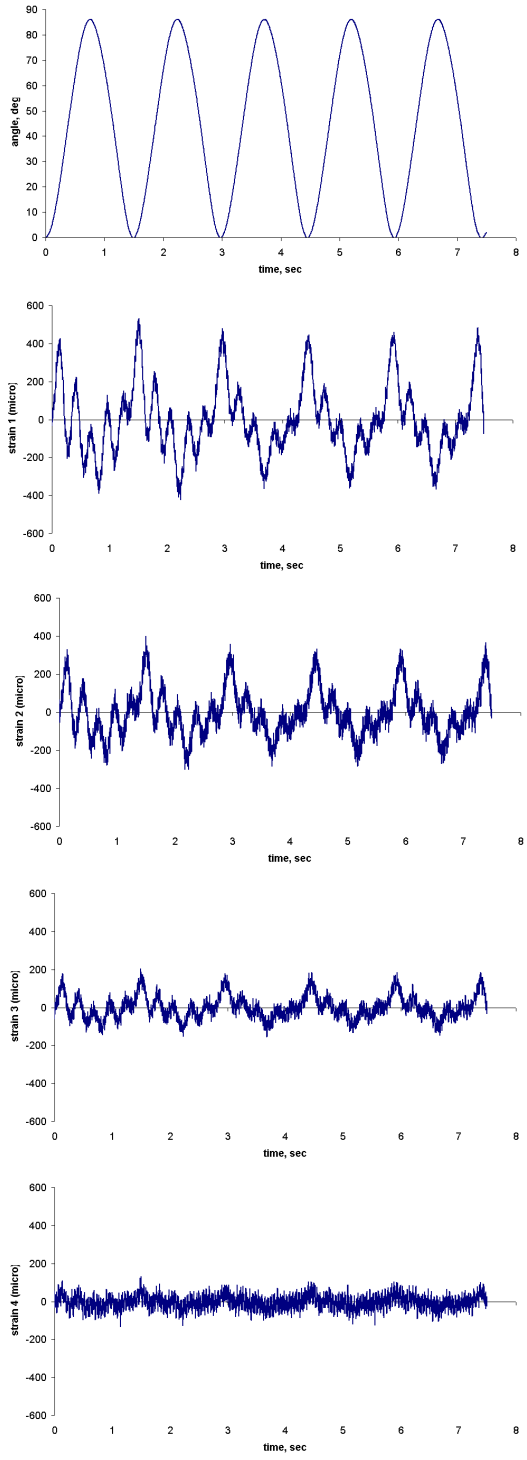

Figure 5: Recorded rotation angle and strains versus time

apparent from the similar shapes of the strain traces, as well as from the FFT plot (Figure 6), that the motion is dominated by the first vibration mode [4]. This provides opportunity for a simplified method for estimating the strains and deformations along the length of the beam.

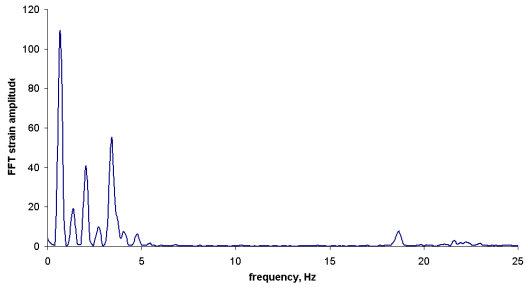

Figure 6: FFT of strain measured at location 1

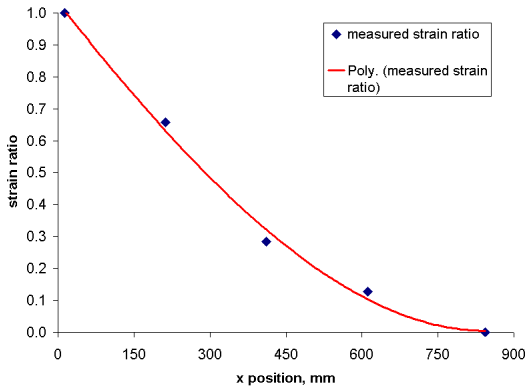

Figure 7: Strain ratio as a function of position along the beam

3.2 Computational Estimate

Quantitative analysis of the time histories of the strains confirm that the strain amplitudes at each of the four strain locations are essentially scaled representations of the strains at the location of strain gauge 1. Consequently, strain ratios are defined such that the amplitudes of strains at locations 2 through 4 are normalized against the amplitude of the strain at location 1. The corresponding values, obtained from least squares analysis, are provided in Table 2. The resulting strain ratios are shown as points in Figure 7. The point at the beam tip is assigned a value of zero as it is known that the end point cannot support a bending moment. Further, the strain ratios are curve fitted using a quadratic polynomial thereby providing an analytical expression for the strains at all locations along the length of the beam.

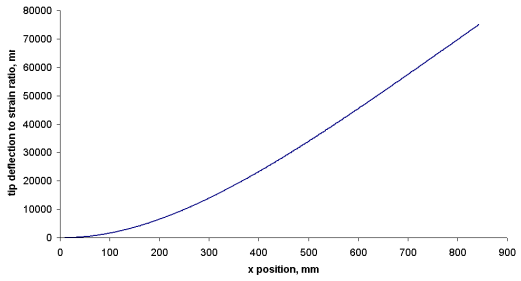

Figure 8: Ratio of the beam tip deflection to the strain measured at location 1

Table 2: Strain scaling ratios as a function of location

Strain	Location, mm	Ratio
1	13	1.00000
2	212	0.65789
3	411	0.28409
4	611	0.12658
end	835	0.00000

The actual strains along the length of the beam are considered to be composed of two parts such that

$$\varepsilon = f(x)s(t) \tag{4}$$

where $f(x)$ is an expression of the scalar strain ratios that are only a function of the point of interest along the length of the beam, and $s(t)$ is the reference strain recorded at the location of strain gauge 1 and is only a function of time.

Interpolation and curve fitting of the strain ratios results in the expression

$$f(x) = 1.042 - (0.2249 \times 10^{-2})x + (0.1200 \times 10^{-5})x^2 \tag{5}$$

where x is the position of interest measured in mm outward along the beam from the inboard end (not the cantilever point).

To obtain curvatures along the length of the beam during its motion, Equation 2 is again used. This results in a continuous expression for the beam curvatures along the length. Double integration with the appropriate boundary conditions

$$\frac{dy}{dx} = 0$$

at the free end x = 835 and

$$y = 0$$

at the cantilever point of the beam at x = 8 mm allows this to be further processed to produce an expression for the beam deflection along its length $Y(x)$ relative to the measured strain

$$\begin{aligned} Y(x) &= (1/1.875)\{(0.1000 \times 10^{-6})x^4 \\ &- (0.3748 \times 10^{-3})x^3 + 0.5211x^2 \\ &- 319.1x + 2.520 \times 10^3\} \end{aligned} \quad (6)$$

where in this case x is measured in mm inward from the tip of the beam.

Using Equation 6 evaluated at the end point of the beam and the measured strain at location 1 it is possible to determine the beam tip deflection. A plot of the ratio of beam tip deflection to the strain measured at location 1 is presented in Figure 8.

3.3 Dynamic Simulation

The ADAMS simulation model of the four-bar linkage and flexible beam was again run, this time for the dynamic conditions that prevailed during the dynamic experiment. The simulated strains at each of the strain gauge locations as well as the tip deflections were output such that they are available for comparison with the directly measured strains and the estimated beam tip deflections.

3.4 Dynamic Results

The measured strains at the location of strain gauge 1, that is used as the reference strain, are compared with the strains predicted by the ADAMS simulation in Figure 9. The strains are compared for a period spanning five cycles in the upper plot and two cycles in the enlarged lower plot. The startup transient exists for roughly the first two cycles of motion. From the results it is evident that the measured and simulated strains are in general agreement.

Next, the estimation approach described in this paper was used to estimate the beam tip deflection as a function of time exclusively from the strain measured at strain gauge location 1. The estimated tip deflection is presented in Figure 10 and the corresponding tip deflection obtained from the simulation is presented in Figure 11. The peak tip deflections predicted by the simulation are approximately 45 mm whereas the peak estimated values reach approximately 50 mm. The oscillation periods are the same in both sets of results. However, the most notable difference is the exaggerated asymmetry resulting from the simulated

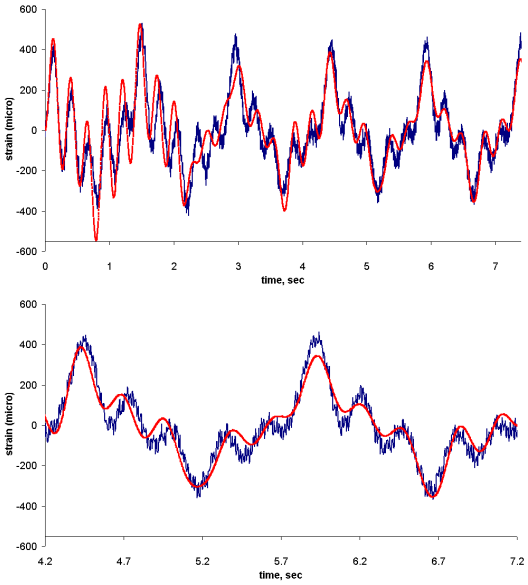

Figure 9: Comparison of measured and simulated strains at location 1 (upper) and corresponding enlarged version (lower)

results compared with the estimated values. As with the strain plots, higher damping in the simulated results is also apparent.

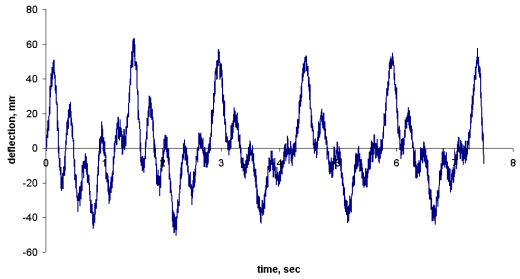

Figure 10: Measured dynamic tip deflection

4 Conclusion and Discussion

The dynamic performance of a flexible beam experiencing reciprocating rotational motion was investigated through experimentation and simulation. The results show that measured strain can be used to estimate the dynamic behaviour along the length of the flexible beam and to predict the tip deflection. Interpolation of the strains lead to an expression for the curvatures of the beam during its motion. This, in turn, could be integrated to obtain the beam deflection profile.

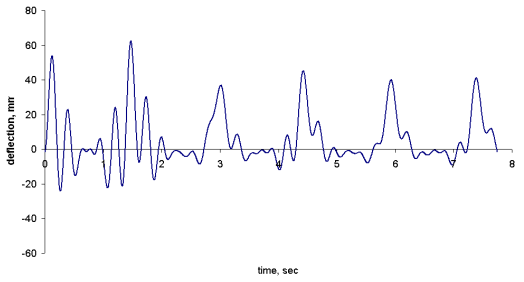

Figure 11: Simulated dynamic tip deflection

With this method, the dynamic properties of the flexible body could be conveniently predicted, thereby providing the opportunity for the flexible body motion to be actively controlled to produce required curvatures of the beam or limiting the tip deflection. Currently, the results presented are limited by the linear assumption of the flexible body and the fact that the excitation primarily affects the first vibration mode of the beam. Preliminary analysis of data corresponding to higher motors speeds demonstrates that a more sophisticated estimation technique is required when more vibration modes are involved in the deformation and when the amplitude of the flexible body deformation is significantly larger.

BIBLIOGRAPHY

[1] A. Higdon and E.H. Ohlsen, *Mechanics of Materials*, Foutth Edition, John Wiley & Sons, New York, 1985.

[2] S.J. Miller and J.C. Piedboeuf, *Estimation of Endpoint Position and Orientation of a Flexble Link Using Strain Gauges*, Proceedings of the Knowlege Based Systems and Robotics Workshop, 1993.

[3] R. R. Craig and M. C. C. Bampton, *Coupling of Substructures for Dynamics Analyses*, AIAA Journal, 6(7), 1968.

[4] W. T. Thomson and M. D. Dahleh. *Theory of Vibration with Applications*, Prentice Hall, Upper Saddle River, 1998.